

Universitat Politècnica de Catalunya

ETSETB

BACHELOR DEGREE IN ENGINEERING PHYSICS

Development of a front hand
interface for a novel Hybrid Detector
for Microdosimetry (HDM)

Author

Mireia Torres Junyent

Supervisor

Chiara La Tessa

Trinitat Pradell



UNIVERSITAT POLITÈCNICA
DE CATALUNYA
BARCELONATECH



June 2021

Abstract

This thesis consist on the design and implementation of a graphic user interface, called MANDARINA. This software is in charge of the data analysis in the read-out system of the Tissue Equivalent Proportional Counter detector (TEPC) in the Protontherapy center in Trento, with which the characterization of the radiation field in a microscopic scale can be achieved. This characterization has a big importance in the radiotherapy field, as it is used in the Treatment Planning System in order to calculate the amount of radiation to apply to cancer patients.

As the detector, MANDARINA is based in the microdosimetry approach. The main functionality of the program is the calculation and representation of microdosimetric distributions and its respective mean values. Also, the program includes interface options, which allows the user to tune the parameters needed in the distribution calculations, among other needs during the experimental sessions with the TEPC.

List of Figures

| | | |
|------|--|----|
| 2.1 | Difference between the range and the track length | 8 |
| 2.2 | Contribution of many little deflection caused by elastic interactions of the incoming particle and the nuclei of the target matter, can result in appreciable changes of direction and scattering angles | 8 |
| 2.3 | Scheme of the abrasion-ablation model. | 9 |
| 2.4 | Bragg curve of C12 for different energies | 10 |
| 2.5 | Typical dose response curves observed for different human tumor cells after irradiation with X-rays. | 12 |
| 3.1 | Energy deposited per unit mass, plotted against the mass m of the scoring volume, as this volume is gradually changed in size. | 13 |
| 3.2 | Calculated microdosimetric spectra, $f(y)$, in a linear representation for energy deposited by 1 MeV electrons in a 1 μm diameter spherical volume. | 17 |
| 3.3 | Log-log representation of the same distribution as in figure 3.2. | 18 |
| 3.4 | $yf(y)$ vs $\log(y)$ representation of the same distribution as in figure 3.2. | 18 |
| 3.5 | Tissue Equivalent Proportional Counter | 19 |
| 4.1 | Experimental set-up in the Protontherapy Center in Trento | 23 |
| 4.2 | Experimental read-out scheme | 23 |
| 4.3 | Experimental read-out in the Protontherapy Center in Trento | 24 |
| 4.4 | Calibration line for set-up configuration | 26 |
| 4.5 | Intercalibration lines for high-medium and medium-low spectrums. | 26 |
| 5.1 | Noise processing of the High Gain spectra | 29 |
| 5.2 | Non-intercalibrated and intercalibrated microdosimetric spectras | 29 |
| 5.3 | Calibrated microdosimetric spectra | 30 |
| 5.4 | Rebinned microdosimetric spectra | 30 |
| 5.5 | Joined microdosimetric spectra | 31 |
| 5.6 | $f(y)$ normalize and $yf(y)$ microdosimetric spectras | 32 |
| 5.7 | $d(y)$ and $yd(y)$ microdosimetric spectras | 33 |
| 5.8 | Interface algorithm scheme | 33 |
| 5.9 | First windows of MANDARINA software. The leftmost photo captures the window in which the user can choose the work space. The rightmost photo captures the pop-up message that the program shows once the work space is selected. | 34 |
| 5.10 | Photos of the data folders and files | 34 |
| 5.11 | Format of the data documents | 35 |
| 5.12 | Photo of the Configuration file in JSON format | 36 |
| 5.13 | Document with the f19 $f(y)$ distribution exported | 37 |
| 6.1 | MANDARINA software | 39 |
| 6.2 | Comparison of normalized $f(y)$ distribution calculated with MANDARINA (right graphic) and with an R code (left graphic) | 41 |
| 6.3 | Comparison of $yd(y)$ distribution calculated with MANDARINA (right graphic) and with an R code (left graphic) | 42 |

Contents

| | |
|---|-----------|
| List of Figures | 2 |
| 1 Introduction | 4 |
| 2 Ionizing radiation | 6 |
| 2.1 Physical processes | 6 |
| 2.1.1 Stopping power | 6 |
| 2.1.2 Scattering | 8 |
| 2.1.3 Nuclear interactions | 8 |
| 2.1.4 Radiation quantities | 9 |
| 2.2 Biological processes | 11 |
| 3 Microdosimetry | 13 |
| 3.1 Theoretical basis | 13 |
| 3.2 Microdosimetry quantites and distributions | 14 |
| 3.3 Representation of Microdosimetric distributions | 17 |
| 3.4 Tissue Equivalent Proportional Counter (TEPC) | 19 |
| 4 Detector and read out | 22 |
| 4.1 Detector | 22 |
| 4.2 Experimental set-up | 22 |
| 4.3 Experimental Read-out | 23 |
| 4.4 Data Analysis | 25 |
| 4.4.1 Calibration | 25 |
| 4.4.2 Intercalibration | 26 |
| 5 MANDARINA | 27 |
| 5.1 Main Goals | 27 |
| 5.2 Programming language | 27 |
| 5.3 Spectra Calculation | 27 |
| 5.4 Interface algorithm | 33 |
| 6 Results | 39 |
| 6.1 Graphic User Interface | 39 |
| 6.2 Analysis of the results | 41 |
| 7 Conclusions | 43 |
| References | 45 |
| Appendices | 47 |

1 Introduction

According to the National cancer institute, radiation therapy (also called radiotherapy) is a cancer treatment that uses high doses of ionizing radiation, to kill cancer cells and control tumors. This treatment is usually applied to patients along with chemotherapy, surgery and/or immunotherapy and over 50% of all patients with localized tumours receive it.

Radiotherapy works by damaging the Deoxyribonucleic acid (DNA) of cells in order to kill them and stop the uncontrolled growth characteristic of cancer tumours. It can be classified in two kinds: Photon radiation (x-rays and gamma rays) and charged particle radiation (electrons, protons, carbon ions, etc). Even if the former kind is the most common technique, particle therapy, and especially proton therapy, is progressively becoming more popular [1]. The interaction of accelerated charged particles with tissue has a different behavior than photons: the physical depth-dose distribution in tissue is characterized by a small entrance dose and a distinct maximum (Bragg peak) near the end-of-range with a sharp fall-off at the distal edges. Whereas the physical depth-dose distribution of photons has the maximum release of dose at the entrance and gradually loses this energy. So, the well defined range and the small lateral beam spread of charged particles, allow to deliver the dose with millimeter precision. Another major advantage of particle therapy is the better sparing of the healthy tissue, which results in a decreased probability of short and long term side effects. However, a major limitation to particle therapy is that the beam delivery is really expensive and technologically challenging, making this technique harder to employ and rising the question whether is cost-effective.

Before patients can undergo an specific radiotherapy treatment, the exact amount of radiation has to be determined and the Treatment Planing System (TPS) is in charge of it. This system relates the physical properties of the incident radiation field (kinetic energy and composition) to the consequent biological effectiveness.

In order to quantify the physical properties of the ionizing radiation needed for the TPS, dosimetry is used as the standard approach. It consists on deterministic and averaged measurements of the dose deposition in volumes of the order of a few centimeters, like standard tumours. However, the most sensitive region to radiation is the DNA of the cells, and at the cellular scale, radiation exhibits a stochastic behaviour, not as in the standard dosimetric macroscopic approach, in which the studied region is large enough to neglect stochastic effects. Microdosimetry, on the other hand, takes into account these fluctuations. This different approach describes and measures the energy deposition of radiation in microscopic volumes, as the dimension scale of cells, and its quantities are microscopic and stochastic. Therefore, in the radiotherapy field, where the incorrect calculations of the applied dose and the estimation of the physical parameters of the beam can produce an underdosing of the tumour or over dosing the healthy tissue, microdosimetry provides, when compared against standard dosimetry, a more accurate approach embedding the radiation quality description at micrometric (cellular) scale.

For these reasons, microdosimetry has gained more importance as it provides a more accurate characterization of the radiation quality at a scale more similar to cells.

This works focuses on the design and implementation of a graphic user interface for real-

time analysis of microdosimetric spectra, acquired with a Tissue Equivalent Proportional Counter (TEPC) in the Protontherapy center in Trento.

Currently, the output signal from the TEPC detector goes through an acquisition chain before being analyzed. This system is composed by multiple amplifiers, as the TEPC signal is very small and negative, by a multichannel analyzer (MCA) which converts the analog signal to digital, and then, by a commercial software MAESTRO (ORTEC) which reads and displays the digital signal. So, the data analysis (calculation of microdosimetric distributions and mean values) has to be done offline with ROOT and R codes. Also, the acquisition system will be soon changed, due to an upgrade of the detector geometry to achieve an improved radiation field characterization. With this improvement, MAESTRO software will be removed and a new program will be needed in order to read the signals coming from the read-out system.

So, the main goals of MANDARINA, the software implemented in this work, are the online microdosimetric analysis of the radiation field, the implementation of the typical characteristics of a graphic user interface to be used at real time (being able to change and tune all the data analysis parameters, visualize the distributions and export the results) and finally, being this new program needed in the future changes of the detector and acquisition chain.

This work is structured in the following parts: first, the basics concepts of ionizing radiation and microdosimetry are illustrated in sections 2 and 3 respectively. Then, the current detector and read-out are deeply commented in section 4 finalizing with the presentation of MANDARINA in section 5, the results in section 6 and the conclusions in section 7.

2 Ionizing radiation

2.1 Physical processes

In this section, the physical processes of charged particles and not conventional gammas, as they act differently, will be explained.

Charged particles are part of the ionizing radiation. When these particles interact with other atoms or molecules with enough energy to exceed a certain energy threshold, secondary particles can be produced such as electrons, releasing energy in the traveling media.

As charged particles travel through the media, two fundamental interaction can occur: electromagnetic and nuclear.

- By *Electromagnetic interactions* the charged particles deposit energy in matter and scatter with the target nuclei and/or the atomic electrons.
- *Nuclear interactions* can cause lateral spread, scattering, in addition to the electromagnetic contribution as well as a loss of the primary ions and production of secondary radiation, nuclear fragmentation.

So, the deposition of energy in matter due to electromagnetic interactions (stopping), the nuclear fragmentation due to nuclear interactions and the scattering due to both kinds of interactions, have to be considered:

2.1.1 Stopping power

In the inelastic interaction with the atomic electrons of the media, the incoming ionized particle transfers an amount of energy to the target material causing excitation (photons, etc) and/or ionization (release of secondary electrons) of the atomic electrons. This is due to the conservation of momentum and energy during collisions.

It results in an energy loss per unit length of the ions, slowing them down, or the *stopping power* S of the media which is described by the Bethe-Bloch equation[2]:

$$S := -\frac{dE}{dx} = \rho \frac{N_A Z}{A} \frac{z_{eff}^2 e^4}{4\pi\epsilon_0^2 m_0 v^2} \left(\ln \left(\frac{Q_{max}}{I(1-\beta^2)} \right) - \beta^2 - \frac{C}{Z} - \frac{\delta}{2} \right) \quad (2.1)$$

All the parameters are described as follows:

- N_a is the Avogadro's number.
- Z is the atomic number for the attenuator, the target material.
- A is the mol weight of the attenuator.
- z_{eff} is the charge of the incoming particle.
- m_0 is the rest mass for the electron.
- v is the velocity of the ionizing particle.

- I is the average ionization potential. This value is theoretical and adjustable.
- Q_{max} is the maximal transferred energy at a single collision ($Q_{max} = 2m_0c^2\beta^2$).
- C is the shell correction.
- δ is the polarization effect.
- β is the incoming particle relative velocity ($\beta = v/c$)

This equation includes some corrections, the shell correction, the density or polarization effect correction and the effective charge correction. The shell correction (C/Z) is for slow particles, when the incident particle velocity is comparable to or smaller than the orbital velocity of the bound electrons (e.g. for protons in the energy range of 1-100 MeV). Can affect the stopping power up to 6%. The density effect correction ($\delta/2$) affect high dense target materials as the electric field seen by the ionizing incoming particles is reduced due to the polarization of the atoms material. It increases with the energy of the particle and reduces the stopping power. The last correction, also called the Barkas-Andersen effect, takes into account the dependence of the incident particle effective charge on its velocity. At high velocities, the atomic electrons are completely stripped off and the ion effective charge is equal to its atomic charge number z . As the ion slows down, ions begin to pick up atomic electrons, reducing even more its velocity and arising the shielding effect. The Barka's empirical formula [3] describes it:

$$z_{eff} = z \left(1 - \exp(-125\beta z^{\frac{2}{3}}) \right) \quad (2.2)$$

From the Bethe-Bloch equation, the following statements can be observed: The stopping power has a quadratic proportionality with the z_{eff} and thus, as charged is the incident particle, more energy will be released. Also, it is inversely proportional to the particle's velocity and consequently, the maximum energy released is reached as the particle is stopping. Another dependency is that the energy released depends on the media properties ($\rho, \frac{Z}{A}$) and finally, that it has a weak dependency with the ionization potential of the media (Q_{max}).

A concept related to this formula is the **range** of the particles in matter. The range is the average path length travelled by a charged particle with kinetic energy E_0 until coming to rest. This value can be well-defined as charged particles lose energy in a quasi-continuous way along their tracks in matter, eventually coming to rest. The equation is the following one:

$$R = \int_{E_0}^0 (dE/dx)^{-1} dE \quad (2.3)$$

It is important to remark that this parameter is different from the track length, as the former is the range of the particles in the media and the last one, the real path of the particles.

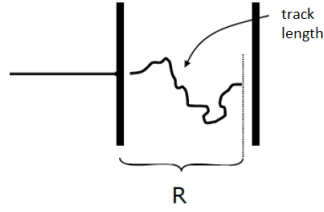


Figure 2.1: Difference between the range and the track length. Illustration from *Radiation: detection and applications* [145888], Corso di Laurea Magistrale in FISICA (LM) of University of Trento.

Another concept related to the Bethe-Block equation is the **range straggling**. This effect is caused by the stochastic nature of the interaction collisions, as ions with the same energy will not stop exactly at the same depth in the medium and thus, the total path ranges of individual particles are spread. These fluctuations are well described for thin absorbers by a Vavilov distribution [4].

2.1.2 Scattering

Besides of slowing down, charged particles can be deflected through electrostatic interactions.

When a charged particle passes close to the atomic nucleus, at a distance much smaller than the atomic radius, the Coulomb interaction is between the fast particle and the nuclear charge rather than with one of the bound electrons. This results in a deflection of the fast particle trajectory and it is called scattering. Each deflection is small and negligible but, the sum of all of the contributions can result in a pronounced change of the particle track.

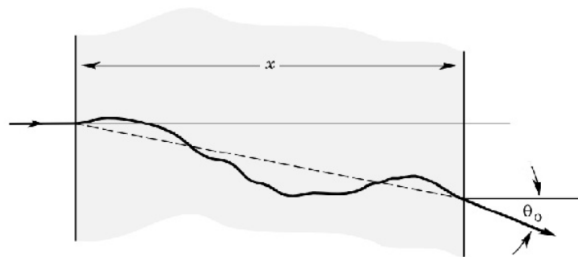


Figure 2.2: Contribution of many little deflection caused by elastic interactions of the incoming particle and the nuclei of the target matter, can result in appreciable changes of direction and scattering angles. From [5].

2.1.3 Nuclear interactions

The nuclear interactions occur at energies of several hundreds of MeV/u. At these energies, violent nuclear spallation reactions may result in a partial or complete desintegration of the incident particle and the target nuclei, being the most frequently interactions the peripheral collisions.

This process is described with the abrasion-ablation model (Serber, 1947)[6] and explained in figure 2.3. As it can be seen in the bellow illustration, the process consist on two steps: The first one is the Abrasion, in which the nucleons contained in the overlapping reaction zone are abraded while the outer nucleons are only slightly affected. And the second one is the ablation. In this step the remaining projectile and target fragments are deexcited by evaporation of nucleons or clusters.

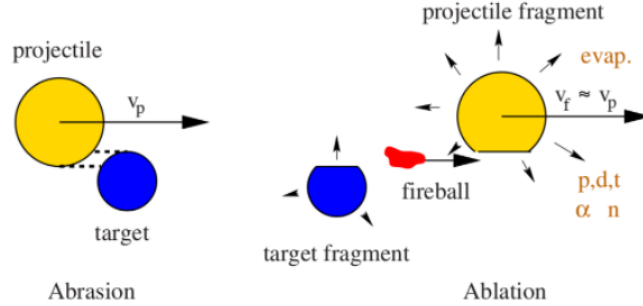


Figure 2.3: Scheme of the abrasion-ablation model. From [7]

These fragmentation reactions can cause a loss of the primary beam particles and a build-up of lower- z fragments, which get more importance as increasing the penetration depth. Also, as these secondary particles move with the same velocity as the primary but with lower z , its range is bigger and can change the depth-energy deposition profile of the primary beam. Therefore, nuclear fragmentation can produce some important effects relevant to radiotherapy with high-energy ion beams.

2.1.4 Radiation quantities

As presented in the introduction of this work, the characterization of the ionizing radiation and the radiation quality are indispensable in order to implement the Treatment Planning System (TPS). This physical characterization of the ionizing field is achieved by the following parameters: The physical absorbed dose D and the Linear Energy Transfer (LET).

Dose

The dose is a macroscopic averaged quantity and it is defined as the fraction of the mean energy imparted by ionising radiation to matter ($d\bar{\epsilon}$) by its mass dm .

$$\bar{D} = \frac{d\bar{\epsilon}}{dm} \quad (2.4)$$

Its unit is the JKg^{-1} , also called Gray, Gy.

All charged particles feature a typical depth-dose profile, called Bragg curve, in which the dose vs the penetration depth of the radiation is described. In figure 2.4, the Bragg curve of C12 for different energies is shown and can be seen that it is divided in five regions:

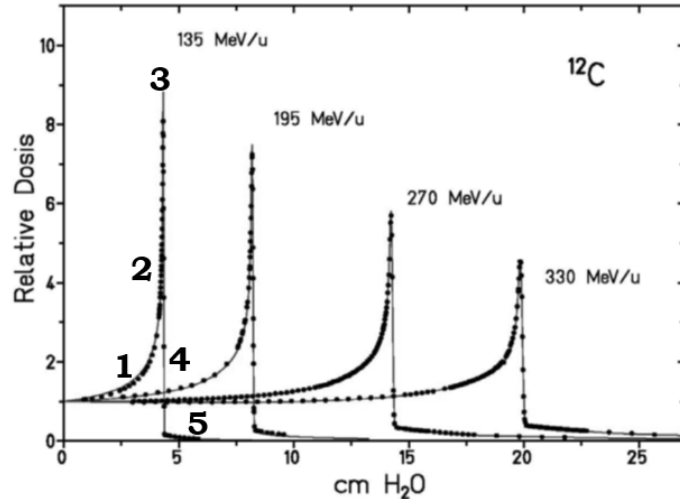


Figure 2.4: Bragg curve of C12 for different energies. Illustration from *Radiation: detection and applications* [145888], Corso di Laurea Magistrale in FISICA (LM) of University of Trento.

1. Plateau: In the entrance region, the dose delivered by the ion is nearly constant due to the constant stopping power at these high energies. Also, in the first few millimetres from the entrance, it is possible to find the production of lower- z secondary particles.
2. Steep rising: As the ion begin to interact with water (first approximation of human body material), the cross section for inelastic reactions increases and thus, so it does the dose, until it saturates.
3. Bragg Peak: It is the maximum dose released by the charged particles and according to Bethe-Block equation (eq. 2.1), it occurs when the ion is stopping.
4. Steep drop after the peak: Once the Bragg peak is reached, the ion is totally stopped and thus, the dose falls off sharply.
5. Tail: As the secondary z -lower particles produced in the entrance region have the same velocity as the primary, they have bigger range which leads to a tail behind the Bragg Peak.

The Bragg curve features changes depending on the ion type and energy. The changes due to different energies can be appreciated in figure 2.4.

Also, if the Bragg curve of multiple mono-energetic ions was described, its Bragg peak would have a width of a few millimeters, not as in the example of figure 2.4. This is due to the range straggling explained in section 2.1.1.

Linear Energy Transfer (LET)

The linear energy transfer (LET) is also an important parameter, as it describes how particles slow down inside the target tissue. Its formula is the infinitesimal ratio between the energy lost by a particle ΔE on a portion of its path Δl :

$$\lim_{\Delta l \rightarrow 0} \bar{L} = L = \left(\frac{dE}{dl} \right) \quad (2.5)$$

Its unit is Jm^{-1} , but it is usually expressed in $\text{keV}\mu\text{m}^2$.

This quantity, as it measures the energy transferred to a medium by charged particles, is related to the stopping power and thus, all the described dependencies coming from the Bethe-Block equation, also happen with the LET. Despite this strong relation, both quantities are quite different, as the LET is defined as the energy imparted by the incoming particle, while S is defined by energy losses of the particle. Moreover LET, is defined in terms of the track length described by the particle as it traverses the medium, whereas stopping power is defined in terms of the thickness of the attenuating medium.

Finally, this quantity is only defined for charged particles, whereas the dose is for all kind of radiation.

2.2 Biological processes

Radiotherapy works by subjecting the cancerous cells to ionizing radiation in order to inactivate them. This is achieved by damaging the Deoxyribonucleic Acid (DNA) of this cells, as it is the most sensitive region to radiation and also, because it carries all of the information to perform cell division.

The cell damage is produced in mainly two ways: the *direct action* is the direct ionization of the DNA molecules and the *indirect action*, consist on the ionization of other molecules which form free radicals, and then ionize the DNA. An example of free radical is the hydroxyl radical (OH^{-1}) coming from the ionization of water molecules inside the cells.

The ionization of the DNA, either by direct action or indirect action, can result in two DNA helix damages, the break of one of its two strands, called *Single strand Break* or both of them, *Double strand break* [8]. Both results in severe outcomes, although the double strand break is more harmful and the single strand break has to be clustered to affect remarkably.

This radiation damage can be quantified with the **Cell survival fraction S**, the fraction of cells surviving after being exposed to specific dose. Basically, it measures the cellular response to the radiation damage and it is modeled as a function of the delivered dose by the Linear-Quadratic (LQ) model:

$$S(D) = \exp(-\alpha D - \beta D^2) \quad (2.6)$$

D is the radiation dose and α and β are experimental coefficients which ratio quantifies the radiosensitivity of the tissue. This ratio has a value of 10 for tumor cells and 2 for normal tissue cells.

An example of survival curves is shown in figure 2.5.

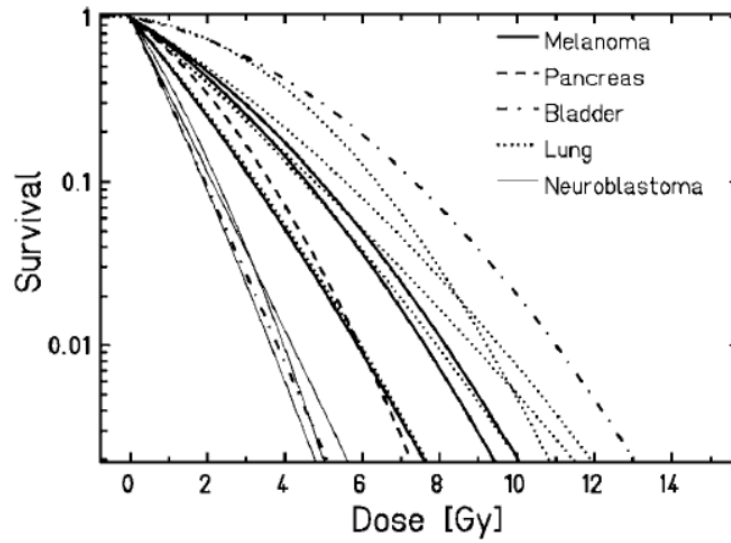


Figure 2.5: Typical dose response curves observed for different human tumor cells after irradiation with X-rays. From [9]

As expected, as the dose increases, the cell survival fraction decreases.

3 Microdosimetry

3.1 Theoretical basis

It is known that ionizing radiation has a stochastic behaviour, as it deposits energy by discrete non-uniformly interactions with the atoms of the target medium. Thus, the average energy deposit per unit mass (absorbed dose), the number of interactions and the magnitude of each energy deposition can all influence the effect of radiation on biological and other structures and therefore, they have to be properly considered.

In enough large target volumes, specifically larger than a few millimeters, the stochastic behaviour can be averaged and thus, the standard and deterministic approach, Dosimetry, can be used. But, in radiotherapy, the most sensitive region is the DNA and then, information of the radiation interaction at a cellular level is needed. At this micrometric scale, the fluctuations in the energy deposition are more relevant and averaged quantities to describe it are no longer reliable. This can be seen in figure 3.1 where m is the enclosed mass in the target volume and E/m the energy deposition per unit mass. Here, as already explained, it can be seen that for large volumes, the absorbed dose D is a correct quantity but not for smaller volumes.

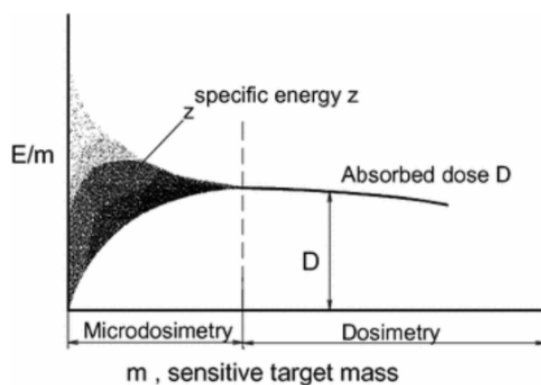


Figure 3.1: Energy deposited per unit mass, plotted against the mass m of the scoring volume, as this volume is gradually changed in size. From [10].

This is why, a different approach is needed.

The microdosimetry approach is a system of concepts as well as of physical quantities and their measurement, which studies the microscopic distribution of energy deposition in irradiated matter. It was originated by Rossi and coworkers.

Historically, this area was developed primarily from a need to understand and quantify the differences in human responses to different types of radiation, in particular the variations in late complications for the same level of acute effects and further applications in radiation health. Also, it arisen in space application, in order to interpret variations in responses of personnel and sometimes electronics to the different radiation fields present in space environments. This is a very important research field as these variations result

in differing risks which must be evaluated for the health and welfare of astronauts and for establishing compliance with regulatory limits [11].

3.2 Microdosimetry quantites and distributions

In microdosimetry, the four fundamental quantities, which are microscopic and stochastic, are the following ones:

Energy deposition

First, the *energy deposition*, ϵ_i , is defined. This quantity measures the energy absorbed at a transfer point, a point where a discrete interaction of the ionizing radiation and matter occurs. It is described as the difference between the energy of the incident ionizing particle (E_{in}) and the energies of all ionizing particles, primary and secondary, leaving the point (E_{out}). The changes of the rest mass energy of all the particles involved are not considered yet so, an extra term is added, $Q_{\Delta m}$. By definition, this last term is positive in a decrease of rest mass and negative otherwise.

$$\epsilon_i = E_{in} - E_{out} + Q_{\Delta m} \quad (3.1)$$

The unit of this quantity is the joule (J) but, can be expressed in the unit eV too.

Energy imparted

Another quantity is the *energy imparted*, ϵ . As its name says, it is the energy imparted to the matter in a volume so, it can be defined as the sum of all the energy depositions in that volume. It is not specific of just one event, defined as the production of statistically correlated transfer points (ex. the track of an energetic charged particle and/or its secondary electrons or the charged particles created in a nuclear reaction) and its formula is the following one:

$$\epsilon = \sum_i \epsilon_i \quad (3.2)$$

It has the same units as the ϵ_i quantity.

Specific energy

The *Specific energy* (imparted), z , is the energy imparted ϵ divided by the mass of the target matter.

$$z = \frac{\epsilon}{m} \quad (3.3)$$

Its unit is the joule per kilogram (Jkg^{-1}) and it is named gray (Gy).

This quantity is related to its probability density $f(z)$, which is the derivative of the distribution function $F(z)$ with respect to z . $F(z)$ is the probability that the specific energy is equal to or less than z .

$$f(z) = \frac{dF(z)}{dz} \quad (3.4)$$

The probability density includes a discrete component at $z=0$ for the probability of no energy deposition.

Then, its expectation value can be calculated. It is called the *Mean specific energy*, \bar{z} , and it is a non-stochastic quantity.

$$\bar{z} = \int_0^{\infty} z f(z) dz \quad (3.5)$$

As z is not specific of just one event, its probability function/density is not either. So, the distribution function of the specific energy deposited in a single event, $F_1(z)$, can be calculated as the conditional probability that a specific energy less or equal to z is deposited if one event has occurred. Its probability density is defined as:

$$f_1(z) = \frac{dF_1(z)}{dz} \quad (3.6)$$

The respective expectation value can be calculated too. In this case, it is called *frequency-mean specific energy per event* and it isn't stochastic.

$$\bar{z}_F = \int_0^{\infty} z f_1(z) dz \quad (3.7)$$

Also, another important probability distribution is the dose distribution of z per energy deposition event. $D_1(z)$ is the fraction of absorbed dose per event delivered by energy deposition events of specific energy less than or equal to z . Its derivative with respect to z , the *dose probability density*, $d_1(z)$, can be calculated as:

$$d_1(z) = \frac{dD_1(z)}{dz} \quad (3.8)$$

The expectation value, the *dose mean specific energy per event*, \bar{z}_D , is a non-stochastic quantity and it is the following one:

$$\bar{z}_D = \int_0^{\infty} z d_1(z) dz \quad (3.9)$$

It exists a relation between $d_1(z)$ and $f_1(z)$ and thus, between its expectation values. These relations are the following ones:

$$d_1(z) = \frac{z}{\bar{z}_F} f_1(z) \quad (3.10)$$

$$\bar{z}_D = \int_0^{\infty} z^2 f_1(z) dz \quad (3.11)$$

Lineal energy

The last quantity is the *Lineal energy*, y , and it is the quotient between the energy imparted (ϵ) by a single event between the mean chord length (\bar{l}), the most probable distance travelled by a particle on a defined geometry. The lineal energy quantity was proposed to replace the LET, a key parameter in describing radiobiological interactions, as a measure of the radiation quality. The reason is that it was proven that averaged quantities didn't provide an accurate representation for highly mixed fields, being the charge particle therapy an example.

The formula is the following one:

$$y = \frac{\epsilon}{\bar{l}} \quad (3.12)$$

The unit of this quantity is the joule per meter (Jm^{-1}), but the most commonly used is $keV\mu m^{-1}$.

The mean chord length \bar{l} for a convex body under a homogeneous and isotropic radiation field is:

$$\bar{l} = \frac{4V}{S} \quad (3.13)$$

where V is the volume and S the surface area of the region[12].

Examples of \bar{l} for different geometries are the following ones:

- Sphere geometry: $\frac{4r}{3}$.
- Cylinder geometry: $\frac{2rh}{r+h}$.

Where r is the radius and h is the cylinder length.

As with the specific energy, it is useful to consider its distribution function and density. The probability density is called the *lineal energy distribution*, $f(y)$, and can be obtained by the derivative of the distribution $F(y)$ with respect to y . Being $F(y)$ the probability that a lineal energy is equal to or less than y .

$$f(y) = \frac{dF(y)}{dy} \quad (3.14)$$

The expectation value is called *frequency-mean lineal energy*, \bar{y}_F , and it is not a stochastic quantity.

$$\bar{y}_F = \int_0^{\infty} y f(y) dy \quad (3.15)$$

The dose distribution of y is important to calculate too. $D(y)$ is the fraction of absorbed dose delivered with lineal energy less than or equal to y and its derivative with respect to y is the *dose probability density*, $d(y)$:

$$d(y) = \frac{dD(y)}{dy} \quad (3.16)$$

The expectation value is called *dose-mean lineal energy*, $\overline{y_D}$, and it is not a stochastic quantity.

$$\overline{y_D} = \int_0^{\infty} y d(y) dy \quad (3.17)$$

By finding a relation between the last two density functions, the expectation value can be re-written. These two equations are the following ones:

$$d(y) = \frac{y}{y_F} f(y) \quad (3.18)$$

$$\overline{y_D} = \frac{1}{y_F} \int_0^{\infty} y^2 f(y) dy \quad (3.19)$$

3.3 Representation of Microdosimetric distributions

The representation of microdosimetric spectra is rarely done in a typical linear plot. This is because $f(y)$ normally takes values that range over 8 order of magnitude and the linear energy can span over very small and large values so, the resultant linear graphic tends to look like figure 3.2.

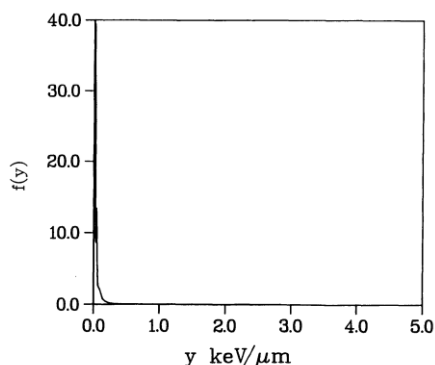


Figure 3.2: Calculated microdosimetric spectra, $f(y)$, in a linear representation for energy deposited by 1 MeV electrons in a $1 \mu\text{m}$ diameter spherical volume. From [13]

This kind of representation gives any visual information of the spectra and thus, other kind of graphics have to be considered.

A log-log plot of the same spectra is shown in figure 3.3. In this case all the details are clearly displayed but, it doesn't provide direct information of the fraction of events per lineal energy as the y-label is in the logarithmic scale.

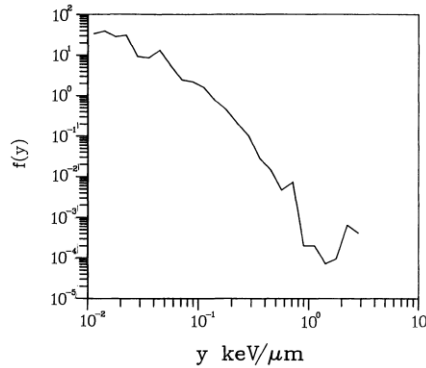


Figure 3.3: Log-log representation of the same distribution as in figure 3.2. From [13]

Therefore, the representation used is the $yf(y)$ vs $\log(y)$. The basis of this is the fact that:

$$\int_{y_1}^{y_2} f(y) dy = \int_{y_1}^{y_2} [yf(y)] d\log(y) = \int_{y_1}^{y_2} [yf(y)] \frac{1}{y} dy \quad (3.20)$$

So, by this representation, all the commented problems are solved. The area under the spectra gives the fraction of events in a direct way and also, all the details are visible in the graphic, as it can be seen in figure 3.4 .

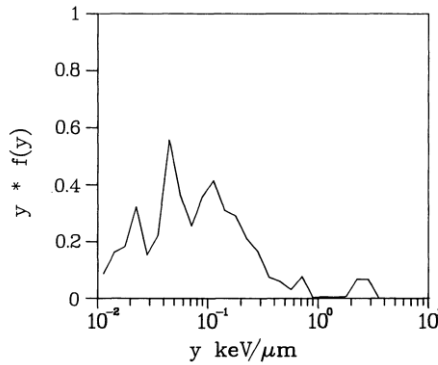


Figure 3.4: $yf(y)$ vs $\log(y)$ representation of the same distribution as in figure 3.2. From [13]

The representation of the other microdosimetric distribution, the dose distribution in y , can be done by plotting $y^2 f(y)$ vs $\log(y)$, as it is proportional to $f(y)$.

Once this convention is done, the expectation values of both distributions can be calculated as follows:

$$y_F = \int_0^\infty y f(y) dy = \frac{\int_0^\infty y^2 f(y) d\log(y)}{\int_0^\infty y f(y) d\log(y)} \quad (3.21)$$

$$y_D = \frac{\int_0^\infty y^2 f(y) dy}{\int_0^\infty y f(y) dy} = \frac{\int_0^\infty y^3 f(y) d\log(y)}{\int_0^\infty y^2 f(y) d\log(y)} \quad (3.22)$$

3.4 Tissue Equivalent Proportional Counter (TEPC)

The main two kinds of detectors in the microdosimetry field are the tissue equivalent proportional counters and the solid state microdosimeters, which purpose is the measurement of the energy deposition in small volumes of the human tissue.

The material of the solid state microdosimeters could be a semiconductor material such as silicon or diamond and its typical sensitive region size can be of the order of the micrometers.

The TEPC is a kind of a proportional counter detector that employs a chamber with tissue equivalent walls and a tissue equivalent fill gas. The chamber can have different geometrical shapes (e.g. spherical, cylindrical, etc) with the typical size of the order of millimeters, with a wire placed inside. Inside this chamber, also called active region, a uniform electric field is applied, the wire being the anode and the wall chambers the cathode.

The work principle of this detector is the following one: When the detector is under a radiation field, the tissue equivalent gas is ionized creating ion-pairs. The electrons, which are related to the energy released and biological damage, are drift by the E-field and collected in the wire producing an electrical pulse. The output signal is very small, of the order of uVs, and its height is proportional to the ionization density of the gas, which at the same time is proportional to the energy deposition due to the incident ionizing particles [14].

In figure 3.5 the TEPC detector is shown. Specifically, it shows the scheme of the active region and the connector box where the signal comes out and the applied High Voltage source comes in to create the electric field.

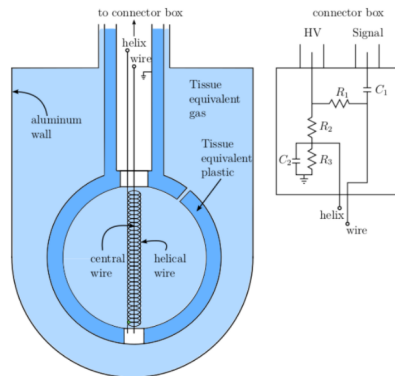


Figure 3.5: Tissue Equivalent Proportional Counter

According to equation 3.12, to calculate the linear energy y from the TEPC measurements, we have to rely on the theoretical mean chord length \bar{l} , the most probable distance travelled by a particle inside the detector. \bar{l} is only valid for homogeneous and isotropic radiation fields and thus, the estimation of this parameter can affect the accuracy of the radiation field quality characterization with this detector.

Another aspect to take into account is that the typical size of the TEPC's active region is of the order of millimeters so, an equivalence with the interested size region (the microscopic volume of biological tissue) has to be reached. To do it, the energy loss in the biological tissue has to be the same as in the gas sphere for equivalent trajectories.

The formula that describes this requirement is the next:

$$\overline{\Delta E}_t = \left(\frac{S}{\rho}\right)_t (D\rho)_t = \left(\frac{S}{\rho}\right)_g (D\rho)_g = \overline{\Delta E}_g \quad (3.23)$$

The t subscript represents the biological tissue and g the tissue like gas. $\overline{\Delta E}_t$ is the mean energy deposited, ρ the density, D the diameter and S/ρ the mass stopping power.

Therefore, to fulfill it and simulate an specific size, the gas density has to be properly chosen.

Besides the biological size equivalence, the biological tissue has to be simulated too by choosing tissue equivalent gasses and wall materials. The requirement to the materials to be tissue-like is that the interaction cross sections and the mass collision stopping power of incident charged particles have to be identical to those of the tissue.

So, generally, the detector is filled with propane-based tissue-equivalent (C_3H_8 -TE) and the standard wall material is A-150 plastic. The A-150 is considered to be muscle equivalent and it is a mixture of polyethylene, nylon, carbon and calcium fluoride.

The fact that the gas and the spherical wall have different densities, as they are different materials, can lead to distortions of the experimental microdosimetric distributions. These distortions are due to the different production of electrons (and particles in general) in both media and thus, if some particles produced on the first media can travel enough to reach the second media, they can produce a perturbation of the actual dose of particles on the second media. This effect is called "Wall effect".

One of the main advantage of this detector is its tissue equivalence, while solid state detectors needs a conversion factor not easy to estimate.

However, its disadvantages are: The limited spatial resolution, as the active region dimension is of the order of millimeters, the wall effects and the pile-up. The pile-up is due to the exposures to high particles rate and can produce spectral distortions. To avoid it as much as possible, the particle rate must be chosen accordingly to the critic pile-up rate of the used TEPC.

Some of the commented TEPC disadvantages are avoided by using the solid state detectors. This is because they offer high spatial resolution (because of the micrometric dimension of its sensitive region, way smaller than TEPC active region scale), information

on the particle charge and the fact that the energy deposition does not suffer the contribution of wall effects. However, they have several limitations too: the sensitive volume is confined in a region of invariable dimensions, the electric noise limits the minimum detectable energy deposition and finally, they require a tissue equivalence conversion, as previously said.

4 Detector and read out

The TEPC detector and its read out, which are being currently used in the Protontherapy Center in Trento, are explained in this section.

4.1 Detector

The detector used in the laboratory is the commercial model type TEPC LET-1/2 from Far West Technology, Inc. Its active region is spherical and made of A-150 tissue-equivalent plastic. The filling gas is pure propane whose pressure is adjusted to reach a density of 1.08×10^{-4} g/cm³. Under these conditions, the detector simulates a tissue-equivalent sphere of 2 μ m diameter. For this TEPC, the mean chord length ($\bar{l} = 4V/S = 4r/3$, being V the volume of the active region, S its surface and r its radius) is $2/3 \cdot 12.7$ mm = 8.47 mm.

4.2 Experimental set-up

The detector is placed inside the experimental room and aligned with the proton beam. This is done with the help of a laser aligning system.

The Tissue Equivalent Proportional Counter, TEPC, is located in the isocenter, the point where the beam is fully characterized. The isocenter is at 125 cm from the exit windows of the beam and within this distance, closer to the TEPC than to the beam exit, the ionization chamber and solid water are usually placed.

The ionization chamber monitors the number of incoming primary ions and the solid water normalizes the beam. The solid water, a water equivalent phantom, is needed because the input beam can be set only to specific energies[15] so, in order to measure different ones, a moderator is needed. Depending on the wanted energy, more or less cm of solid water must be placed along the beam line. Specifically, the wider the solid water is, the beam is slowed more down and thus, lower energies are reached. This is translated in higher energy depositions inside the TEPC, since slower ions deposits more energy (Equation 2.1).

A photo of the experimental set-up in the protontherapy center in Trento is shown in figure 4.1. The furthest device is the ionizing chamber and the closest one is the solid water. The TEPC is not placed and aligned yet but, as it will be seen in next section photo, it is normally situated on top of the blue structure, at the isocenter.



Figure 4.1: Experimental set-up in the Protontherapy Center in Trento

4.3 Experimental Read-out

The experimental read out of the TEPC detector in the Protontherapy center is shown in the following scheme:

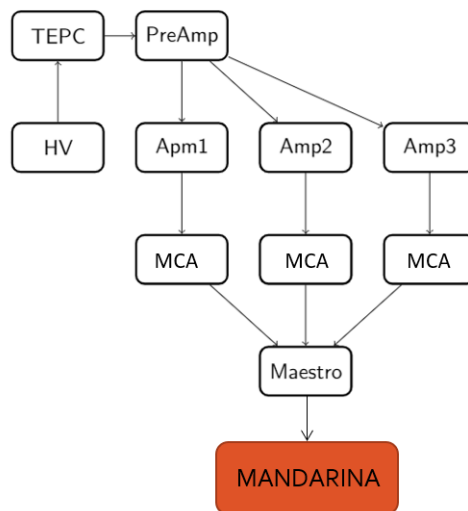


Figure 4.2: Experimental read-out scheme

The TEPC is connected to a pre-amplifier[16], the amplifier in charge of extracting the signal from the detector without significantly degrading the intrinsic signal-to-noise ratio. The main functionalities of the pre-amplifier is to change the polarization of the input signal as it is of hundreds of uV negative shaped (the signal consist on an electron's flow) and apply a first small gain. The connection of the detector with this device is done by a short coaxial cable in order to expose the less the unprocessed signal to the room noise. Also, to avoid the experimental noise, the pre-amplifier is placed inside an isolating box.

Next, it is connected to three amplifiers[17] with different gains. This is due to the fact that the signal dynamic range is huge[13] so, if only one gain was used, or the low values wouldn't be enough amplified or the higher would saturate.

Another aspect to take into account is that the gain settings have to be chosen in such a way that every two neighboring spectra (ex. the one coming from the High Gain amplifier and the other from the medium) have an overlapping region so that they can be matched to give the total spectrum without any gap, and the total spectrum has to cover the whole energy range. Therefore, the three gains used are $G \sim 10, 100, 1000$.

Then, the three amplifiers are connected to three multichannel analyzers (MCAs) where the electrical signal is converted to a digital signal. Specifically, the MCA analyzes the output voltage pulses coming from the amplifiers and sorts them into a histogram, or "spectrum" of number of events, versus pulse-height. This spectrum is visualized and recorded with MAESTRO (ORTEC) [18], a data acquisition system and finally, are processed with MANDARINA software and $y_f(y)$, $y_d(y)$ and the mean values are calculated.

The read out in the experimental room of the Protontherapy center in Trento is shown in figure 4.3. In the right photo it can be seen the TEPC and the isolating box that contains the preamplifier and in the left photo, the high voltage source, the three amplifiers and the MCA's. Although it doesn't appear in these photos, the MCA's are connected to a computer where MAESTRO is installed. Then, using AnyDesk, this computer is connected remotely to another in the control room. MANDARINA is used in this other computer.

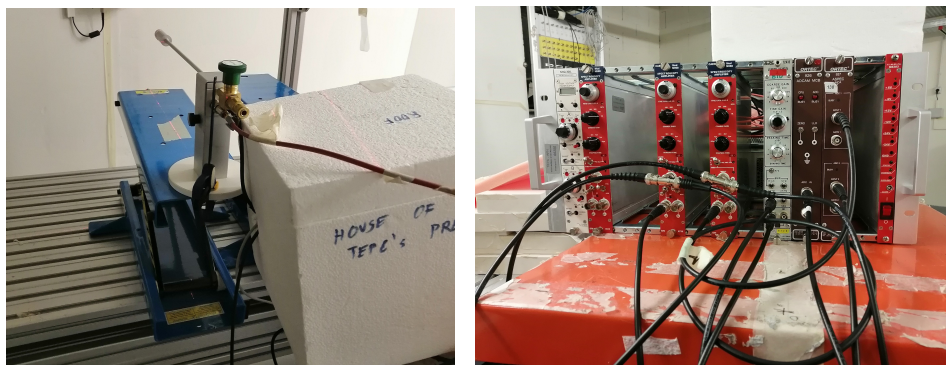


Figure 4.3: Experimental read-out in the Protontherapy Center in Trento

The model of the devices of the read-out are the following:

- The pre-amplifier is a Camberra 2006 (03759).
- The source of HV is a NHQ 102n (2kV).
- The amplifiers are INTERTECHNIQUE 7243E for the High and Medium Gain and TENNELEC TC243 for the Low Gain.
- The MCA's for the High and Medium Gain are Multi Channel Analyzer model 927 by ORTEC.

- The MCA for the Low Gain is a Multi Channel Analyzer model 926 by ORTEC.

And, the typical configuration of the devices (amplifier shaping time, the HV source and number of channels) are chosen in order to reduce as much as possible the ambient noise and to maximize the signal resolution [19].

4.4 Data Analysis

As explained above, the last step of the experimental read-out and set-up is done with MANDARINA software. The software mainly merges the spectra resulting from the different amplifier gains in one spectrum. In order to achieve it, the MCA channels have to be calibrated to lineal energy y and an intercalibration between the three different gain spectras has to be done.

In this section, the basis of these two processes will be explained.

4.4.1 Calibration

The calibration is done with the help of a Monte Carlo code and the points taken into account are from the peak of the $f(y)$ spectra (due to protons mean energy deposition) and the proton edge.

The aim of this approach is to do a Monte Carlo simulation with the same parameters of the experiment and obtain the simulated experiment spectra. In this case, instead of having the x-axis in terms of channels, it is in terms of linear energy (y). This process is done for a unique nominal beam energy and repeated for different solid water width. The reason for this is that protons deposit very small energies ($\sim 0.5 \text{ keV}/\mu\text{m}$ with a energy of 70 MeV) and this spectra region has a lot of ambient noise. Thus, in order to obtain reliable points, the peak of the $f(y)$ spectra, the most probable energy deposition due to protons, has to be shifted to higher energies. This is achieved by adding solid water along the beam, therefore reducing the protons energy.

Then, a comparison between the peaks of the simulated and the measured spectra can be done.

However, this procedure doesn't give information of the whole channels range, as adding solid water just shifts the peak energy deposition to values of few $\text{keV}/\mu\text{m}$ and thus, it is impossible to span the whole $f(y)$ spectra. Therefore, the proton edge is used too. The proton edge is the value of y associated to the maximum energy that a proton can release in the TEPC by stopping at the distal edge. This value does not depend on the protons itself, just on the detector and can be theoretically calculated by knowing the detector geometry and the gas composition[20]. It is easily estimated with Monte Carlo [21].

Once all the necessary points are obtained, experimentally and by the simulation, the relation y -channels can be calculated. This relation is a second order function. And, although the quadratic term is small, it is necessary as it depends on the non linearity of the electronic response, which is expected at the edge of the electronic range and on the detector due to second order effects.

The calibration depends on the chosen experimental set-up (shaping time of the amplifiers, voltage of the HV source, etc) so, each time any of the commented parameters is changed, the calibration has to be changed too.

Figure 4.4 shows the Calibration line for a set-up of $2\mu\text{s}$ of shaping time and 700V of High Voltage. The line coefficients are written in equation 5.5.

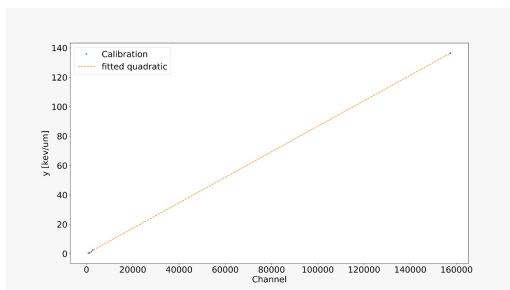


Figure 4.4: Calibration line for set-up configuration

4.4.2 Intercalibration

The intercalibration consist on finding a lineal relation between the channels of the three spectra in order to plot them together in one merged graphic.

To obtain the linear relation, a pulser-generated signal is sent to the different MCA's and the channels corresponding to the same voltage signal are plotted one against the other. This procedure is done repeatedly, changing the voltage signal amplitude and finding different points to make the linear relations more exact. Then, a linear regression of all the founded points is done and the coefficients of the intercalibration lines are finally calculated.

The intercalibration depends on the gains of the amplifiers so, each time they are changed, the relation has to be found again.

The intercalibration lines for $G \sim 10, 100, 1000$, used set-up, can be seen in figure 4.5 and the corresponding formulas are equations 5.3 and 5.4.

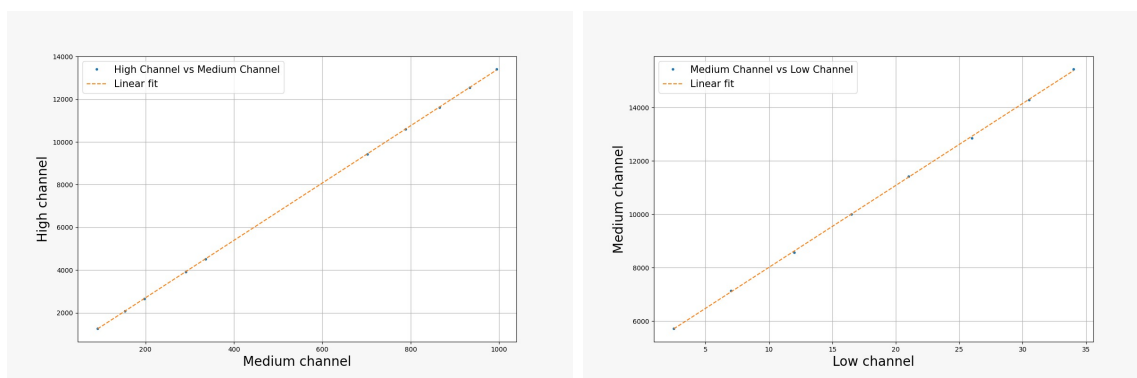


Figure 4.5: Intercalibration lines for high-medium and medium-low spectrums.

5 MANDARINA

5.1 Main Goals

MANDARINA software is a real-time graphic user interface that calculates typical microdosimetric spectra and mean values in order to characterize the radiation field obtained with the TEPC detector. So, it must include a: data acquisition & analysis and everything needed to tune data analysis parameters, graphic visualization and exportation, etc.

Regarding the acquisition & analysis, data require a processing in order to reconstruct the microdosimetric spectra. Moreover, noise play an important factor especially in the high-gain amplifiers, requiring specific strategies implementation to achieve minimal spectra distortion.

5.2 Programming language

To develop the graphic user interface, C# and Labview were considered because they are a good tool for this application. Also, because MAESTRO only supports the Microsoft Windows operating system and therefore, the program should do it too. In the future case where MAESTRO will be no longer used, the chosen operating system is equally useful as most of the used computers in the laboratory have this OP.

Other reasons were that I already knew Labview, as it is worked in one degree's subject, and in the C# case, that it was a new language for me and thus, a good opportunity to learn object-oriented programming discipline and a new tool.

Finally, MANDARINA uses C# with the 4.8 .NET Framework [22]. The chosen Framework [23] allows the interface to plot all of the wanted spectrums, use JSON (JavaScript Object Notation) and REGEX (Regular expressions) among other needed tools.

5.3 Spectra Calculation

In order to reconstruct all of the microdosimetric spectra with MANDARINA, the following programming steps have to be done:

Every graphic of this section represents the data corresponding to the following experiment:

- Nominal energy of the proton beam: 148 MeV.
- A depth in water of 130 mm and 100 mm lateral with respect the beam line.

And the set-up of the read-out devices are:

- The source of High Voltage is set to 700 V.
- The shaping time of the amplifiers is $2\mu\text{m}$.
- The MCA's corresponding to the High and Medium Gain signal are of 4096 channels.

- The MCA corresponding to the LowGain signal is of 1024 channels.

Time factors

Every time that a measurement is done, the MCA takes some time to convert the electrical input signal to an output digital signal. During this time, no more events can be acquired and thus, information from the detector is lost. Then, two variables can be defined, the *Real time*, r , and the *Life time*, l . The first indicates all the measuring time and the second, only the time that the MCA's are acquiring.

So, to take into account all of the events of the experiment, all the MAESTRO output data have to be multiplied by a factor. This factor, f , is different for each amplifier files. Then, as the noise measurements are not taken at the same time and same duration that the radiation data, the noise have to be multiplied by another factor, f_2 .

$$f = \frac{r}{l} \quad (5.1)$$

$$f_2 = \frac{r}{r_{noise}} \quad (5.2)$$

Noise processing

The experimental room, where the TEPC and the acquiring electronic chain are placed, has a lot of ambient noise and therefore, so does the acquired data.

To process this noise, the following approaches are made: the measured noise is subtracted from the energy deposition data and then, the resultant spectra is cut off in a certain channel.

In the picture below, this method is described for the High Gain spectra. First, the noise and the data are plotted together and it can be seen that the big peak is just noise and not measured events, although it cannot be totally appreciated in the graphic. The next plot shows the spectra once the subtraction has been done and a big peak can still be observed. This is noise yet so, a cut off value must be chosen to remove it. This value also avoids the creation of negative channels, negative y's, with no physical meaning. In this case, the cut off value is channel 80.

Finally, the last chart shows the spectra with the noise processing done.

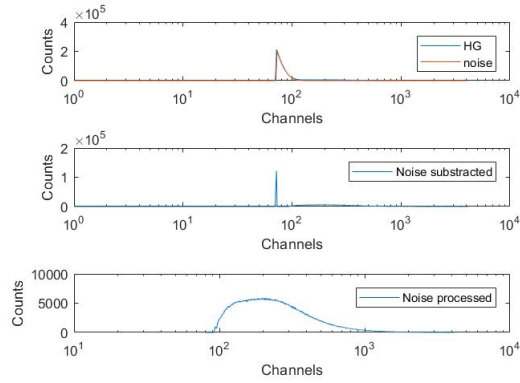


Figure 5.1: Noise processing of the High Gain spectra

Intercalibration

Then, the intercalibration is performed and an idea of the resultant spectra can be firstly appreciated.

The Low Gain spectra has very small values in comparison with the other spectrum and this is why it cannot be properly seen in figure 5.2.

The intercalibration lines used in this graphic are:

- Calibration medium to high:

$$\text{HighCh} = 10.49 \cdot \text{MediumCh} - 27.44 \quad (5.3)$$

- Calibration low to medium:

$$\text{MediumCh} = 79.36 \cdot \text{LowCh} + 1391 \quad (5.4)$$

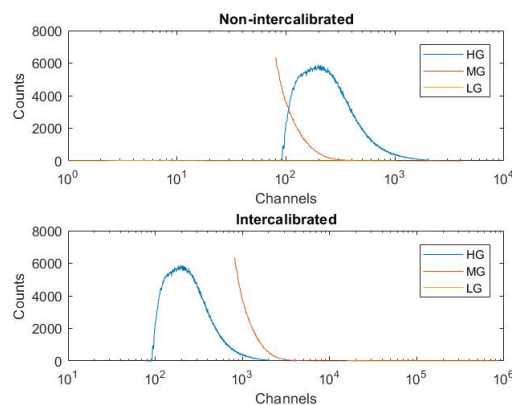


Figure 5.2: Non-intercalibrated and intercalibrated microdosimetric spectras

Calibration

In the calibration step, the conversion of channels to y 's is done. As explained in the background section, it is achieved by applying a specific second order function to the channels.

Figure 5.3 shows the calibrated spectra and the calibration line used is :

$$y [\text{Ch}] = -7.10683224 \cdot 10^{-8} \cdot \text{Ch}^2 + 0.0025 \cdot \text{Ch} + 0.0509 \quad (5.5)$$

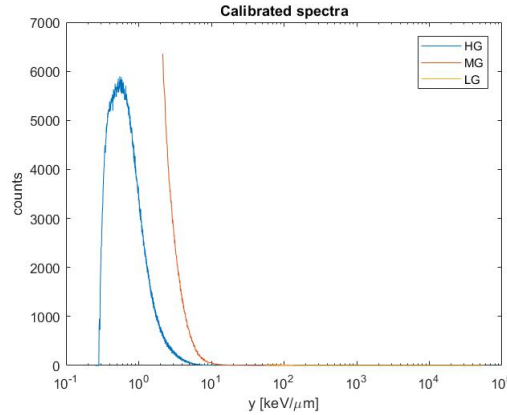


Figure 5.3: Calibrated microdosimetric spectra

Rebinning

Because of a Microdosimetric convention, all of the histograms have to be plotted in a specific way, they must have 100 bins and the y value between (0.1,1000) logarithmically spaced. So, the y vector has to be re-written in order to fulfill these two conditions and then, the counts vector has to be reorganized with respect to it. As one bin is an interval of lineal energies, to reorganize the counts vector, a summation of counts per lineal energy inside each bin has to be done. This procedure is called rebinning.

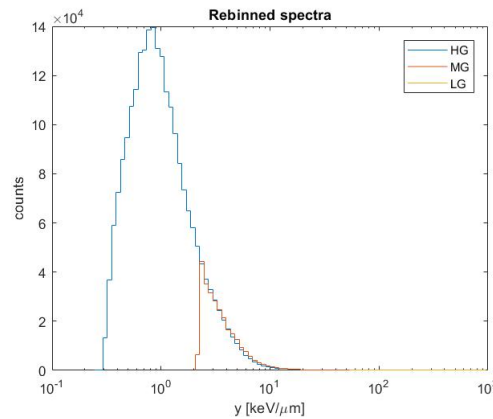


Figure 5.4: Rebinned microdosimetric spectra

Joining

As the three spectra have been obtained by three different amplifier gains, they have not the same shape height but they are related proportionally. This is why it is necessary to make them equivalent. To achieve this, an y joining point is selected which belongs to both histograms (for the medium-high and low-medium joining). Next, the averages for the two neighboring spectra of the counts vector point corresponding to the selected y and some previous and posterior points is performed. And finally, a ratio between these two factors can be done and applied to one of the two spectra to join. An average is performed and not a single point is considered, in order to avoid problems in the case of a very sharp and peaky spectra, which can lead in a bad calculation of the proportional factor. Usually, the calculated factors are applied to the High Gain data, in the medium-high merge, and to the low gain, in the low-medium merge. This is due to the fact that the medium gain data is the most reliable one as the high gain amplifies a lot of noise and the low gain shape is very peaky.

Also, the selected joining point is in charge of cutting off again the unmerged spectra. As it can be seen in figure 5.3 and 5.4, the HG and MG spectra have an overlapping region and, although it is not appreciated it, the MG and LG spectra have it too. Therefore, the user has to decide which spectra is more reliable (HG-MG merge and MG-LG merge) in these regions in order to delete the overlapping and achieve a whole continuous spectra. This is done by the joining point, as it will be where the High Gain data will be cut off and the medium Gain will begin for the high-medium merge and the same for the medium-low.

Figure 5.5 shows the merged spectra using the following joining points and interval:

- High-Medium: 5 [keV/um] and interval of 2 bins.
- Medium-Low: 100 [keV/um] and an interval of 1 bin.

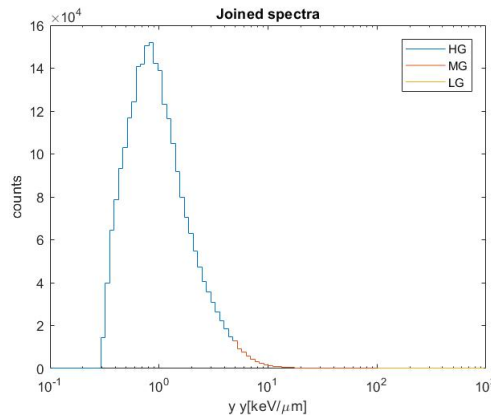


Figure 5.5: Joined microdosimetric spectra

Normalization

Next, the merged spectra has to be normalized by two factors, the bin width and the area under the histogram curve.

The purpose of normalizing the spectra by the first factor is to eliminate the dependence with it, since the bigger/smaller is the bin width, more/less counts will be stored there. The second factor is to convert the counts to a probability distribution.

The area under the curve is calculated with the ICRU R36 [24] approach and its demonstration is shown in appendix 1.

$$\int_0^{\infty} yf(y) d\log(y) \simeq \sum_{i=0}^{\infty} \frac{\ln(10)}{B} y_i f(y_i) \quad (5.6)$$

With $B = \frac{1}{\Delta(\log(y))}$.

f(y), yf(y), d(y), yd(y) and mean values

Finally, the spectrum and the mean values can be calculated.

The f(y)'s spectra is obtained directly from the previous normalization. Then, it is multiplied by the linear energy in order to have yf(y). Next, this spectra is normalized by its area, obtaining the d(y) and lastly, is multiplied by y. In this last step yd(y) is calculated. Once the program has calculated them, the mean values are computed using formulas 3.21 and 3.22 by the ICRU report 36 approach (equation 5.6).

In the following figure all of the obtained histograms are plotted:

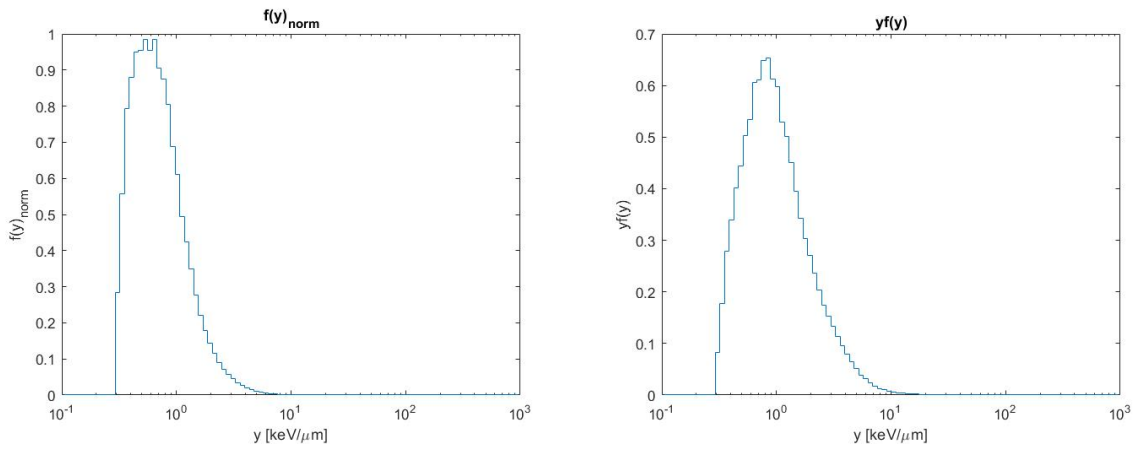


Figure 5.6: f(y) normalize and yf(y) microdosimetric spectras

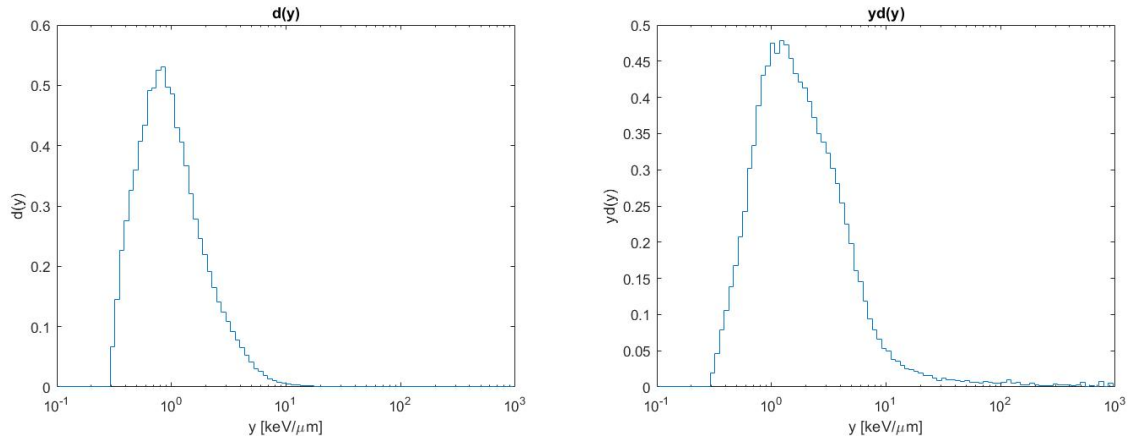


Figure 5.7: $d(y)$ and $yd(y)$ microdosimetric spectras

5.4 Interface algorithm

The algorithm of MANDARINA is the following one: First, it gives the option to the user to choose the work space, the folder which contains all of the measurement files. Then, the configuration parameters such as the coefficients of the intercalibration and calibration files are automatically upload. These first values are default and can be changed later. The next step is to read and process all of this data in order to calculate the microdosimetric spectrum and quantities. And finally, the distributions are plotted, the mean values are shown and they are exported in a .txt file.

In the next scheme the interface flow is shown:

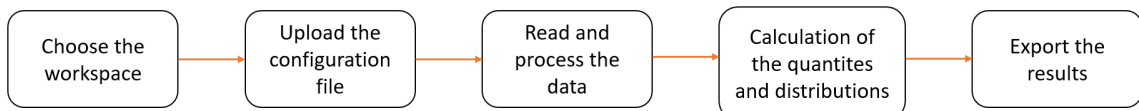


Figure 5.8: Interface algorithm scheme

However, in order to make the program as robust and accessible as possible to the users, there are more steps between the principal ones. The whole procedure is explained in detail below:

Choose the workspace

First, a pop up window of the computer's file system appears in which, manually, the user can choose the folder that contains the data that wants to process. In figure 5.9 the pop-up window is shown along with a confirmation message.

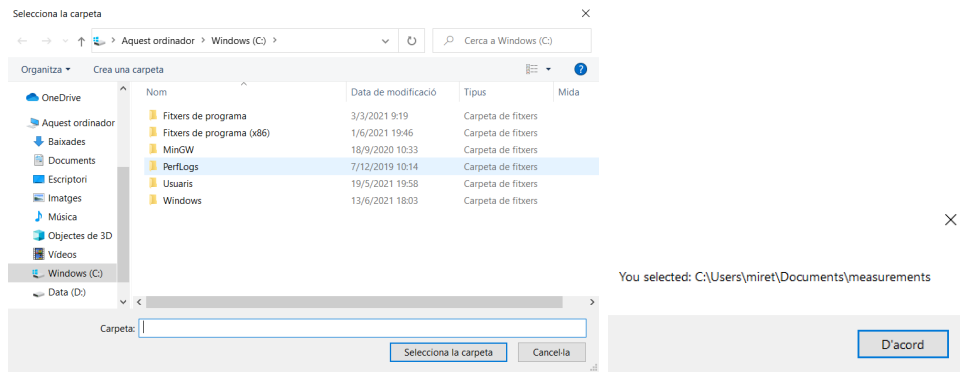


Figure 5.9: First windows of MANDARINA software. The leftmost photo captures the window in which the user can choose the work space. The rightmost photo captures the pop-up message that the program shows once the work space is selected.

The format of the folder is the one that the researchers are currently using and it is the following one:

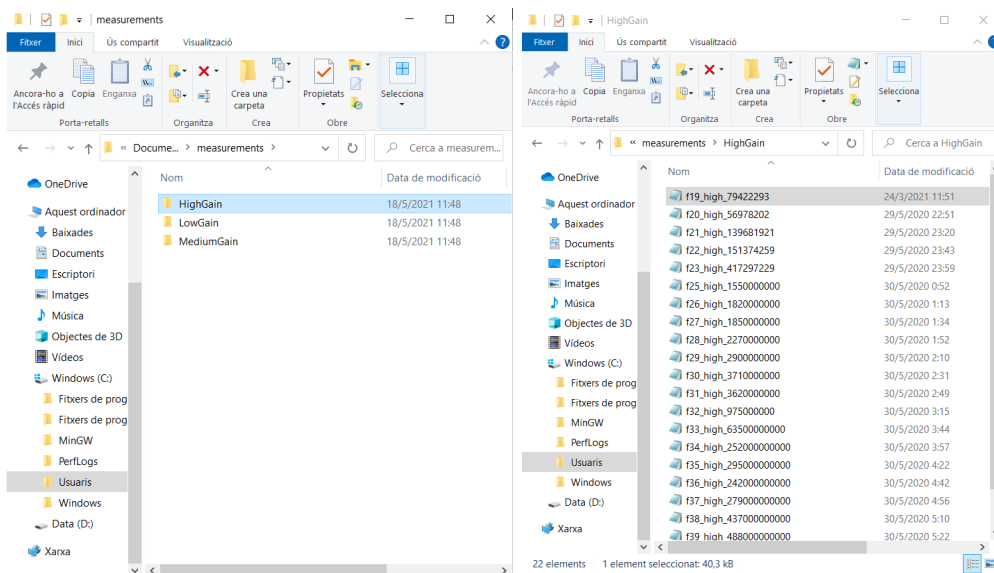


Figure 5.10: Photos of the data folders and files

As it can be seen, there is a main folder that contains three more. In each of these folders the data coming from the three amplifiers (High Gain, Medium Gain and Low Gain) are stored in .SPE files. They are numerated and every three files with the same number, each of them coming from the different gain folders, corresponds to one measurement.

Check the files

In order to construct a spectra, first, the user has to choose which measurement wants to analyze and thus, which number. Then, the program can begin to calculate the spectra by processing the three data files and the three noises.

- Coefficients of the Calibration curve.
- Cut off values for the High Gain, Medium Gain and Low Gain data.
- Joining points (HG-MG and MG-LG).
- Interval of the joining points.

As explained in the introduction of this subsection, once MANDARINA starts, it automatically uploads a default values of these parameters. The default values are saved in a JSON string format in a text file called ConfigurationFile.

JSON, JavaScript Object Notation, is a text format for storing and transporting data. This format is very useful because it uses human-readable text to store and transmit data objects consisting of attribute–value pairs and arrays. In the interface code, it is processed by serializing and deserializing the string contained in the files.

In the below figure, the ConfigurationFile with this structure is shown:



Figure 5.12: Photo of the Configuration file in JSON format

Later in the program, the user has the possibility to change these parameters directly from the interface and save them in new text files. Also, to choose another existing file instead of the default document.

The interface always shows the name of the used configuration.

Spectra Calculation

All of the calculations required to obtain the microdosimetric distributions ($f(y)$ and $y_d(y)$) and its mean values are performed in this step of the code.

Chart

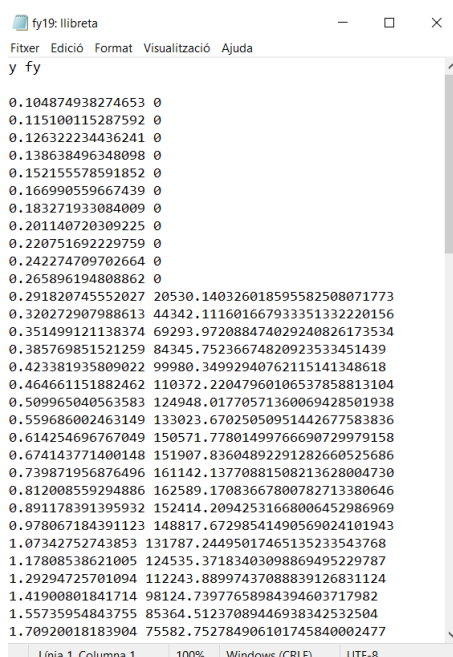
Next, the software plots $f(y)$, normalized $f(y)$, $yf(y)$, $d(y)$ and $yd(y)$ in different charts placed in different tabs of the interface. The $f(y)$ graphic is plotted in two ways, showing the three separated data (HG, MG and LG) and merged.

Also, it shows the calculated mean values in another tab.

Export the Data

Finally, all of the calculated data is exported in text files. This can be achieved by two ways, exporting all of the distributions at the same time or one by one.

The format of the resultant documents is: the file's name is the data's name (f_y , yf_y , etc) along with the measurement number and has the next structure:



```
fy19: llibreta
Fitxer Edició Format Visualització Ajuda
y fy
0.104874938274653 0
0.115100115287592 0
0.126322234436241 0
0.138638496348098 0
0.152155578591852 0
0.166990559667439 0
0.183271933084009 0
0.201140720309225 0
0.220751692229759 0
0.242274709702664 0
0.265896194808862 0
0.291820745552027 20530.140326018595582508071773
0.320272907988613 44342.11160166793335133220156
0.351499121138374 69293.972088474029240826173534
0.385769851521259 84345.75236674820923533451439
0.423381935809022 99980.34992940762115141348618
0.464661151882462 110372.22047960106537858813104
0.509965040563583 124948.01770571360069428501938
0.559686002463149 133023.67025050951442677583836
0.614254696767049 150571.77801499766690729979158
0.674143771400148 151907.83604892291282660525686
0.739871956876496 161142.13770881508213628004730
0.812008559294886 162589.17083667800782713380646
0.891178391395932 152414.20942531668006452986969
0.978067184391123 148817.67298541490569024101943
1.07342752743853 131787.24495017465135233543768
1.17808538621005 124535.37183403098869495229787
1.29294725701094 112243.88997437088839126831124
1.41900801841714 98124.73977658984394603717982
1.55735954843755 85364.51237089446938342532504
1.70920018183904 75582.752784906101745840002477
Línia 1. Columna 1 100% Windows (CRF) UTF-8
```

Figure 5.13: Document with the f19 $f(y)$ distribution exported

Also, a folder is created in the document environmental user path. It is called "DataFiles + the date" and is the place where the exported files are saved.

Besides doing these principal steps and functionalities, MANDARINA has a few other options to make the real-time analysis easier to the user.

- It gives the option to see the configuration parameters (cut off values and joining points).
- The chosen work space can be changed whenever the user needs to and not only at the beginning of the program.

- It can acquire the data from the new measurements in a real-time way by clicking a refresh button in the interface.
- Can handle errors and "exceptions" that may occur during the running of the software. This errors can be the wrong selection of the input files, the configuration parameters, etc.

6 Results

6.1 Graphic User Interface

MANDARINA graphic user interface is the following one:

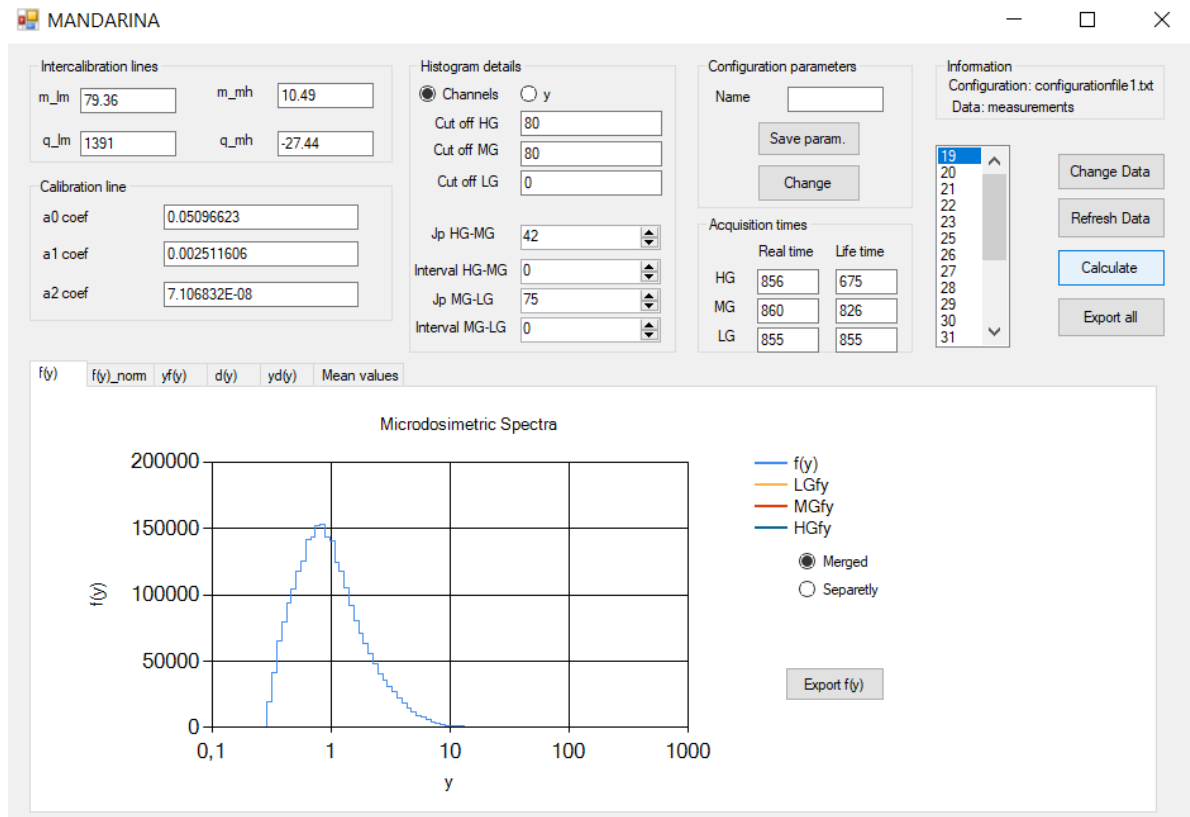


Figure 6.1: MANDARINA software

As it can be seen in figure 6.1, the interface is divided in two main areas. The upper zone is where all the needed data and parameters can be selected and changed along with other functionalities. Whereas in the bottom, all the distributions are plotted and the mean values are shown.

The rightmost upper area have all the commands that let the user choose which Data wants to process. First, in the upper right corner, the information box shows the name of the selected work space and of the configuration file used. Below this, a large scroll box shows all the available measured data (19, 20, 21, etc) of the selected work space, as the program first checks which numbers (measures) have all the necessary files to calculate the distributions (explained in section 5.4). Once the user clicks a number, MANDARINA automatically process the data, calculate and represent all the microdosimetric distributions and mean values. Also, the Acquisition times box shows the real and the life time, the measuring time and the acquiring time correspondingly, of the data (HG for the High Gain data, MG for the Medium Gain and LG for the Low Gain). Next to the scroll box and below the information box there are 4 buttons:

- Change Data: This button let the user change the work space whenever it is needed.
- Refresh Data: By clicking this button, the software acquires the new measured data. This button avoids the re-initialization of the program every time that a new measure is taken, as the principal MANDARINA algorithm only reads new data at the beginning.
- Calculate: Once it is pressed, the program calculates and shows all the distributions and quantities. This button is useful because during the analysis of the data, sometimes it is necessary to change the cut off values and the joining point in order to obtain the best spectra as possible. The criterion, as explained in section 5.3, is to subtract the noise from each different gain spectra and do a proper joining.
- Export all: This button exports all the calculated quantities in a .txt file.

The left upper area shows the intercalibration lines, calibration line and histogram details boxes. These boxes are automatically filled in the beginning of the program execution, as the default parameters are upload from the basic configuration file (explained in section 5.4).

The first two boxes shows the coefficients of the intercalibration and calibration equations and let the user change them by clicking on and writing directly in it. They are labeled in the following way:

- Medium to high intercalibration:

$$\text{HighCh} = m_{mh} \cdot \text{MediumCh} - q_{mh} \quad (6.1)$$

- Low to medium intercalibration:

$$\text{MediumCh} = m_{lm} \cdot \text{LowCh} - q_{lm} \quad (6.2)$$

- Calibration:

$$y[\text{Ch}] = a2coef \cdot \text{Ch}^2 + a1coef \cdot \text{Ch} + a0coef \quad (6.3)$$

The Histogram details shows the cut off values for the three unmerged spectra (cut off HG, cut off MG and cut off LG), the joining points (Jp HG-MG and Jp MG-LG) and the intervals (Interval HG-MG and Interval MG-LG) needed to calculate the ratio for the joining. The cut off values can be changed in the same way as the coefficients and the joining points and intervals by clicking the up and down buttons. The program doesn't let the user choose any value and the only eligible points are previously calculated in order to asses the choice of logical and possible points and not random, which can cause errors in the code.

The user can choose to see these parameters in terms of channels or in terms of lineal energy y , by clicking the radio button "Channels" or "y". In figure 6.1 all the parameters are shown in terms of channels.

Finally, the Configuration parameters box let the user the following:

- If the parameters are changed, they can be saved in a new Configuration File. In order to do it, the user has to write the name of the file in the Name box and then click the save param. button.
- All the configuration parameters can be changed at once by clicking the Change button. Once it is pressed, a window appears and the user can choose which file wants to upload. Then, the parameters are automatically actualized.

The calculated spectra and mean values are shown in the bottom area. As it can be seen in the above figure, the graphics are ordered in tabs. In each tab there are: an export button, in case the user only wants to export one distribution and not all of them, the graphic (the lineal energy in the x axis and the distribution in the y axis), its legend and in the case of the $f(y)$ spectra, two radio buttons. These buttons give the option to represent the merged $f(y)$ or to see the three spectra (HG, MG and LG). The Mean values tab only shows dose-mean lineal energy $\overline{y_D}$ and the frequency-mean lineal energy $\overline{y_F}$.

6.2 Analysis of the results

In order to asses the functionality of the program, two tests have been done:

First, the spectra calculation has been checked. To do it, the microdosimetric spectra and mean values of the f19th data have been calculated with MANDARINA and with the off-line R code developed and used to process the data offline. This data corresponds to the experiment in section 5.3. Then, both spectra have been plotted side by side to check if they are equal, meaning that the program works, or not, meaning that it doesn't.

The graphics are shown in figures 6.2 and 6.3.

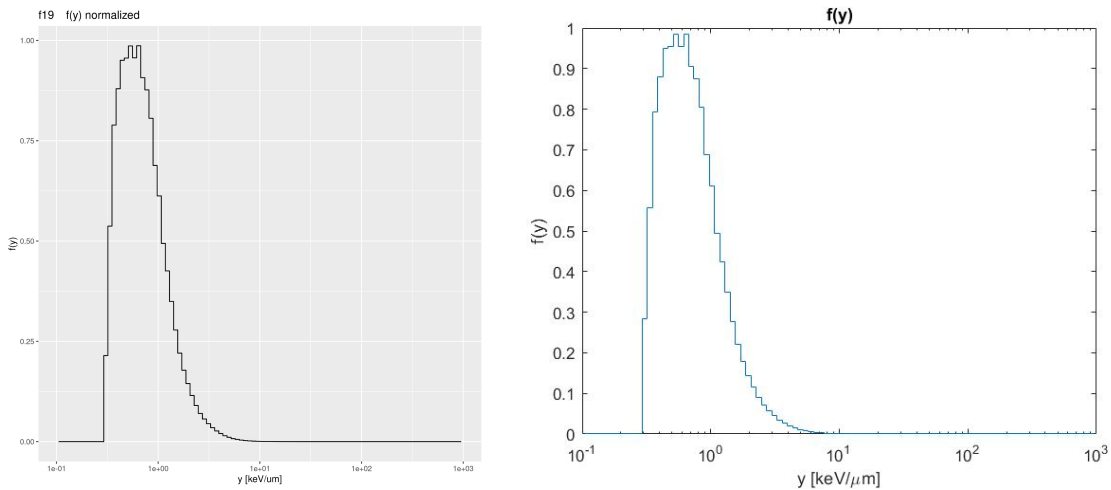


Figure 6.2: Comparison of normalized $f(y)$ distribution calculated with MANDARINA (right graphic) and with an R code (left graphic)

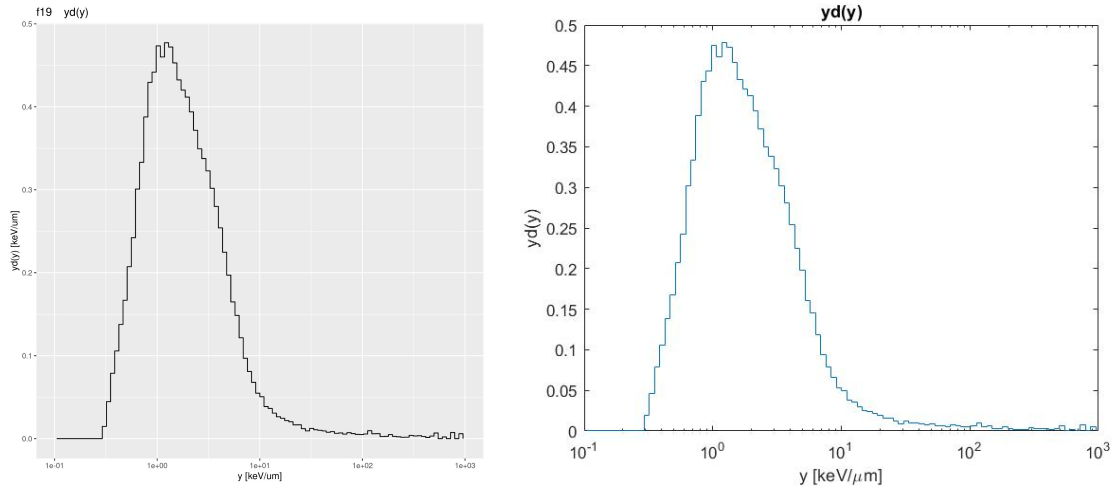


Figure 6.3: Comparison of $yd(y)$ distribution calculated with MANDARINA (right graphic) and with an R code (left graphic)

It can be seen that for each distribution, both spectra are the same so, MANDARINA works correctly.

Finally, the software has been tested in the ProtonTherapy Center in Trento too. The setup used was the one described in section 4.3, taking the measurements in the experimental room and acquiring them with MAESTRO, which computer was connected remotely to a computer in the control room with MANDARINA software, which analyzed the data and calculated the spectra. From this session, the program showed some shortcomings (e.g. not being able to change the work space while the program is being executed, etc) that were improved later. These improvements are already explained in sections 5 and 6.1.

7 Conclusions

In radiotherapy, the characterization of the ionizing radiation field provides information to implement the Treatment Planning system (TPS), a software that calculates the dose distribution to apply to patients. This characterization can be approached by two systems, Dosimetry and Microdosimetry. The former is the standard approach and it is based in macroscopic and averaged measures and quantities while, the last one consist on stochastic and microscopic measurements. As the most sensitive region of the cancer tissue is the DNA of cells, the target interactions of the radiation are at cellular (micrometric) scale and thus, the standard approach is not enough accurate. This is due to the fact that at this low volumes, the stochastic behaviour of ionizing radiation cannot be averaged and therefore, stochastic quantities to describe it are needed. Because of this, microdosimetry is becoming more popular.

In order to quantify the physical properties of the radiation, microdosimetric detectors are used. In the Protontherapy Center in Trento, Tissue Equivalent Proportional Counter detector (TEPC) is used along with an acquisition chain. The goal of the acquisition chain is to make the output signal from the detector suitable for its analysis, as the signal is negative and of the μV scale order. The change of the polarization of the signal is achieved by a preamplifier, which also adds a small gain, and it is the first device in the read-out. Then, the signal passes through three amplifiers with different gains ($G \sim 10, 100, 1000$ for the Low gain, the Medium gain and High gain amplifiers respectively) in order to finally amplify the signal. The reason of using three different gains is due to the fact that the detector signal dynamic range is huge [13] and using only one amplifier with one specific gain doesn't give a good signal to be processed. Then, three multichannel analyzers (MCAs) convert the three analogical signals (each one coming from one of the amplifiers) to a digital signals and MAESTRO (ORTEC), records and displays them. MAESTRO is mostly for nuclear physics application and it is not specified in the Microdosimetry field. So, to further process the data, the calculation of the microdosimetric distributions and mean values has to be done offline and with an external code. Because of this, a new software is needed to process directly and at real time, all the data coming from the read-out.

In this work, this software has been programmed and implemented. MANDARINA is a real-time graphic user interface in C# that calculates typical microdosimetric spectra ($f(y)$, $yf(y)$, $d(y)$ and $yd(y)$) and its mean values (the frequency-mean lineal energy, $\overline{y_F}$, and the dose-mean lineal energy, $\overline{y_D}$). It includes a data acquisition & analysis, spectra calculation and representation, the exportation of the results and many features and options in order to be useful and easy to manage by any user during the experimental sessions. The functionality of the software is explained in sections 5 and 6.

Finally, MANDARINA was tested with good results in the Proton Therapy center in Trento.

The future improvements of the detector and its read-out will consist on the replacement of the TEPC detector by an Hybrid detector for microdosimetry (HDM), the MCA's for a FPGA board, a hardware circuit, and the rid off of the MAESTRO software.

HDM is an hybrid detector that uses a TEPC to measure the energy imparted ϵ and a

Low Gain Avalanche Detectors-based tracker (LGAD), a silicon solid state detector, to measure the real track of the ionizing particles. The main advantage of this new detector with respect to the TEPC, is the substitution of the theoretical mean chord length \bar{l} , the most probable distance travelled by a particle in a volume, for the real track in the lineal energy calculation (equation 3.12). This way, the inaccuracy due to the estimation of \bar{l} , which is only valid for homogeneous and isotropic radiation fields, is avoided and a more accurate characterization of the ionizing radiation can be done.[26]

The read-out prospective changes are because the analog data, which has a lot of relevance in this measures, is lost with the current electronic chain. So, the FPGA board and the rid off of MAESTRO, which is a blackbox, will allow a more flexible data acquisition as the whole time series will be analysed. With these improvements, MANDARINA will be in charge of the data reading and analysis and thus, its current code will have to be slightly changed in order to implement it.

References

- [1] Loeffler and Durante. Charged particle therapy-optimization, challenges and future directions. *Nature Reviews Clinical Oncology*, 10:411–424, 2013.
- [2] H. A. Bethe. Molière’s theory of multiple scattering. *Phys. Rev.*, 89:1256–1266, Mar 1953.
- [3] W.H. Barkas and D.A. Evans. *Nuclear Research Emulsions: Techniques and theory*. Academic press, 1963.
- [4] Edward L. Alpen. *Radiation Biophysics, Second edition*. Academic Press, 2013.
- [5] Meroli Stefano. Multiple scattering for particles in matter. https://meroli.web.cern.ch/lecture_multiple_scattering.html.
- [6] R. Serber. Nuclear reactions at high energies. *Phys. Rev.*, 72:1114–1115, Dec 1947.
- [7] Riccardo Ridolfi. Study of the track reconstruction in the foot experiemtn for hadron-therapy. *PhD thesis*, 2018.
- [8] KK Khanna and SP Jackson. Dna double-strand breaks: signaling, repair and the cancer connection. *Nature genetics*, 27(3):247—254, March 2001.
- [9] M Scholz. *Microdosimetric response of physical and biological systems to low-and high-LET radiations*. Elsevier, 2006.
- [10] H.H. Rossi. *Microscopic Energy Distribution in Irradiated Matter*. Academic Press New York, 1968.
- [11] C. La Tessa, S. Guetersloh, L. Heilbronn, J. Miller, L. Sihver, and C. Zeitlin. Fragmentation of 1gev/nucleon iron ions in thick targets relevant for space exploration. *Advances in Space Research*, 35(2):223–229, 2005. Space Life Sciences: Ground-Based Iron-Ion Biology and Physics, Including Shielding.
- [12] N.G. Sjöstrand. What is the average chord length? *Annals of Nuclear Energy*, 29:1607–1608, 2002.
- [13] H.H. Rossi and M. Zaider. *Microdosimetry and Its Applications*. Springer berlin Heidelberg, 2012.
- [14] Sabina Chiriotti, Davide Moro, Paolo Colautti, Valeria Conte, and B Grosswendt. Equivalence of pure propane and propane te gases for microdosimetric measurements. *Radiation protection dosimetry*, 166, 05 2015.
- [15] F. Tommasino, M. Rovituso, S. Fabiano, S. Piffer, C. Manea, S. Lorentini, S. Lanzone, Z. Wang, M. Pasini, W.J. Burger, C. La Tessa, E. Scifoni, M. Schwarz, and M. Durante. Proton beam characterization in the experimental room of the trento proton therapy facility. *Nuclear Instruments and Methods in Physics Research Section A: Accelerators, Spectrometers, Detectors and Associated Equipment*, 869:15–20, 2017.
- [16] ORTEC. Preamplifier introduction. <https://www.ortec-online.com/-/media/ametekortec/other/preamplifier-introduction.pdf?la=en>.

- [17] ORTEC. Introduction to amplifiers. <https://www.ortec-online.com/-/media/ametektortec/other/amplifier-introduction.pdf?la=en>.
- [18] Maestro multichannel analyzer emulation software. <https://www.ortec-online.com/products/application-software/maestro-mca>.
- [19] Glenn F. Knoll. *Radiation Detection and Measurement, 4th edition*. John Wiley & Sons Inc, 2010.
- [20] Davide Moro, Sabina Chiriotti, Valeria Conte, Paolo Colautti, and B Grosswendt. Lineal energy calibration of a spherical tepec. *Radiation protection dosimetry*, 166, 04 2015.
- [21] D. Moro, S. Chiriotti, V. Conte, P. Colautti, and B. Grosswendt. Lineal energy calibration of a spherical TEPC. *Radiation Protection Dosimetry*, 166(1-4):233–237, 04 2015.
- [22] Bill Wagner. .net documentation. <https://docs.microsoft.com/en-us/dotnet/>.
- [23] Dotnet. .net framework documentation. <https://docs.microsoft.com/en-us/dotnet/framework/>.
- [24] International commission on radiation units and measurements. *Microdosimetry, ICRU REPORT 36*. Springer berlin Heidelberg, 1983.
- [25] Dotnet. Regex class (system.text.regularexpressions). <https://docs.microsoft.com/en-us/dotnet/api/system.text.regularexpressions.regex?view=net-5.0>.
- [26] M. Missiaggia, E. Pierobon, M. Castelluzzo, A. Perinelli, F. Cordoni, M. Centis Vignali, G. Borghi, E. V. Bellinzona, E. Scifoni, F. Tommasino, V. Monaco, L. Ricci, M. Boscardin, and Chiara La Tessa. A novel hybrid microdosimeter for radiation field characterization based on the tissue equivalent proportional counter detector and low gain avalanche detectors tracker: A feasibility study. *Frontiers in Physics*, 8:472, 2021.
- [27] National cancer institute. Radiation therapy for cancer. <https://www.cancer.gov/about-cancer/treatment/types/radiation-therap>.
- [28] Philip Mayles, Alan Nahum, and Jean-Claude Rosenwald. *Handbook of radiotherapy physics. Theory and Practice*. CRC Press 1 edition, 2007.
- [29] Marco Zaider and Harald H. Rossi. *Microdosimetry and Its Application to Biological Processes*, pages 171–242. Springer US, Boston, MA, 1986.

Appendices

ICRU Report 36 demonstration

By definition, the probability density $f(y)$ is normalized to 1 energy deposition event:

$$\int_0^{\infty} f(y) dy = 1 \quad (.1)$$

As it has been demonstrated in section 3.3, the first and second following terms are equivalent. Then, by using the logarithm property $\ln x = \ln 10 \cdot \log x$ the third term can be found too.

$$f(y)dy = yf(y)d(\ln y) = (\ln 10)yf(y)d(\log y) \quad (.2)$$

The logarithmic scale of y can be subdivided in B increments per decade, and its n th value is:

$$y = y_0 10^{\frac{n}{B}} \quad (.3)$$

where y_0 is the lowest value of y . Next, the logarithm increment of y can be calculated as follows:

$$\Delta(\log y) = \frac{1}{B} \quad (.4)$$

If B is large enough, the integral .1 can be discretized as a sum and dy can be replaced by formula .4.

$$\int_0^{\infty} f(y) dy = \int_0^{\infty} yf(y) d(\log y) \approx \frac{\ln 10}{B} \sum_{i=0}^{\infty} y_i f(y_i) = 1 \quad (.5)$$

JSON Configuration file code

The *c#* code implemented in order to generate the default Configuration file, explained in section 5.4. A variation of this code is also used in MANDARINA main program code.

```
using System;
using System.Windows.Forms;
using System.Text.Json;
using System.IO;

namespace ConfigurationFile
{
    public partial class Form1 : Form
    {
        public Form1()
        {
            InitializeComponent();
        }
        public class Intercalibr
        {
            public double mlm { set; get; }
            public double qlm { set; get; }
            public double mmh { set; get; }
            public double qmh { set; get; }
        }
        public class Calibr
        {
            public double a0 { set; get; }
            public double a1 { set; get; }
            public double a2 { set; get; }
        }
        public class Conf
        {
            public double cutoffHG { set; get; }
            public double cutoffMG { set; get; }
            public double cutoffLG { set; get; }
            public Intercalibr intercalibr { set; get; }
            public Calibr calibr { set; get; }

            public Conf()
            {
                this.cutoffHG = 80; this.cutoffMG = 80; this.
cutoffLG = 0;
            }
        }
    }
}
```

```

        Intecalibr intercalibrobj = new Intecalibr();
        intercalibrobj.mmh = 10.49; intercalibrobj.qmh =
-27.44;
        intercalibrobj.mlm = 79.36; intercalibrobj.qlm =
1391;
        this.intercalibr = intercalibrobj;

        Calibr calibrobj = new Calibr();
        calibrobj.a0 = 0.05096623;
        calibrobj.a1 = 0.002511606;
        calibrobj.a2 = 7.106832e-8;
        this.calibr = calibrobj;
    }

}

private void Serialization_Click(object sender,
EventArgs e)
{
    Conf Cf = new Conf();
    string jsonString = JsonSerializer.Serialize(Cf);
    File.WriteAllText(@"C:\Users\miret\Documents\tfg\
measurements\configurationfile1.txt", jsonString);
}
}
}

```